EUROPEAN ORGANIZATION FOR NUCLEAR RESEARCH

April 15, 2009

2008 PROGRESS REPORT ON PS215/CLOUD

University of Innsbruck, Institute of Ion Physics and Applied Physics, **Austria**
University of Vienna, Institute for Experimental Physics, **Austria**
Institute for Nuclear Research and Nuclear Energy, Sofia, **Bulgaria**
University of Tartu, Department of Environmental Physics, Tartu, **Estonia**
Helsinki Institute of Physics and University of Helsinki, Department of Physics, **Finland**
Finnish Meteorological Institute, Helsinki, **Finland**
University of Kuopio, Department of Applied Physics, **Finland**
Tampere University of Technology, Department of Physics, **Finland**
Goethe-University of Frankfurt, Institute for Atmospheric and Environmental Sciences, Frankfurt am Main, **Germany**
Leibniz Institute for Tropospheric Research, Leipzig, **Germany**
University of Lisbon, Department of Physics, **Portugal**
Lebedev Physical Institute, Solar and Cosmic Ray Research Laboratory, Moscow, **Russia**
CERN, Physics Department, **Switzerland**
Fachhochschule Nordwestschweiz (FHNW), Inst. Aerosol & Sensor Technology, Brugg, **Switzerland**
Paul Scherrer Institut, Laboratory of Atmospheric Chemistry, **Switzerland**
University of Leeds, School of Earth and Environment, **United Kingdom**
University of Reading, Department of Meteorology, **United Kingdom**
Rutherford Appleton Laboratory, Space Science & Particle Physics Departments, **United Kingdom**
California Institute of Technology, Division of Chemistry and Chemical Engineering, **USA**

CLOUD Collaboration

CERN-SPSC-2009-015 / SPSC-SR-046
06/05/2009
CERN-SPSC-2009-015 / SPSC-SR-046
15/04/2009

1 INTRODUCTION

The CLOUD experiment aims at a quantitative investigation of the potential link between galactic cosmic rays and climate. It is an interdisciplinary experiment that integrates the heritage of particle physics detectors with state-of-the-art instruments developed for the analysis of ions, trace gases, aerosols, water droplets and ice particles in the atmosphere.

During 2008 the CLOUD activities have mainly involved completion of the analysis of the data from the 2006 beam run with the pre-CLOUD experiment (§2), modifications to the T11 experimental zone, and design and construction of the CLOUD-09[1] chamber and instrumentation (§3). These activities are summarised in this document, together with the 2009 schedule and beam request to commission CLOUD-09 and begin the first physics measurements (§4).

Since the time of the 2006 pre-CLOUD experiment at CERN, five new groups have joined the CLOUD collaboration (Institute for Nuclear Research and Nuclear Energy, Sofia; Fachhochschule Nordwestschweiz, Brugg; U Innsbruck; U Lisbon and U Tartu) and two groups have departed: DTU, Copenhagen, and (owing to the retirement of Prof. F. Arnold) MPIK, Heidelberg. In addition, 10 Marie Curie fellows have recently joined the CLOUD-ITN partner institutes, funded with 2.4 M€ over a three year period by the EU FP7. Of the ten fellows, 8 are Ph.D. students who will carry out their thesis research on CLOUD-09 and 2 are postdocs.

[1]The name *CLOUD-09* is chosen to signify the first year of operation of the chamber rather than a state of happiness.

2 RESULTS FROM THE 2006 PRE-CLOUD EXPERIMENT

The results reported here have been prepared as a draft manuscript for submission to *Atmos. Chem. Phys.*

2.1 Summary

During October–November 2006, an experiment was performed at the CERN PS in preparation for CLOUD. The purpose of the pre-experiment was firstly to carry out exploratory measurements of the effect of ionising particle radiation on aerosol formation from trace H_2SO_4 vapour and secondly to provide technical input for the CLOUD design. Around 50 nucleation bursts were observed, with formation rates of particles above the 3 nm detection threshold of between 0.1 and 100 $cm^{-3}s^{-1}$, and growth rates between 2 and 37 $nm\,h^{-1}$. The corresponding H_2SO_4 concentrations were typically around 10^6 cm^{-3} or less. The experimentally-measured nucleation rates and H_2SO_4 concentrations are comparable to those found in the atmosphere, supporting the idea that sulphuric acid is involved in the nucleation of atmospheric aerosols. However, sulphuric acid alone is not able to explain the observed rapid growth rates, which suggests the presence of additional trace vapours in the aerosol chamber, whose identity is unknown. By analysing the charged fraction, a few of the aerosol bursts appear to have a substantial contribution from ion-induced nucleation and ion-ion recombination to form neutral clusters. Some indications were also found for the accelerator beam timing and intensity to influence the aerosol particle formation rate at the highest experimental SO_2 concentrations of 6 ppb, although none was found at lower concentrations. Overall, the exploratory measurements provide suggestive evidence for ion induced nucleation but the experimental variables were neither sufficiently well controlled nor sufficiently reproducible to quantify the conditions under which ion processes become significant. Finally, concerning technical aspects, the most important lessons for the CLOUD design include the stringent requirement of internal cleanliness of the aerosol chamber, as well as maintenance of extremely stable temperatures ($<0.1^{\circ}$C).

2.2 Background

In its Fourth Assessment Report, 2007, the Intergovernmental Panel on Climate Change (IPCC) attributes more than 90% of the observed climate warming since 1900 to the rise of anthropogenic greenhouse gases in the atmosphere [IPCC (2007)]. Aerosols and clouds are recognised as representing the largest uncertainty in the current understanding of climate change. The IPCC estimates that changes of solar irradiance (direct solar forcing) have made only a small (7%) contribution to the observed warming. However, large uncertainties remain on other solar-related contributions, such as the effects of changes of ultraviolet (UV) radiation or galactic cosmic rays on aerosols and clouds [Carslaw, Harrison and Kirkby (2002), Lockwood and Fröhlich (2007), Kazil, Harrison and Lovejoy (2008), Enghoff and Svensmark (2008)] [Kirkby (2007)]. So far, no quantitative estimates of galactic cosmic ray-induced changes in aerosol and cloud formation have been reached. Experiments are planned for the CERN CLOUD facility to resolve this discrepancy [CLOUD Collaboration (2000, 2004, 2006)].

The concept of CLOUD is to construct a large aerosol chamber in which conditions anywhere in the atmosphere can be recreated and then to expose the chamber to a particle beam at CERN, which closely replicates natural cosmic rays. The chamber is equipped with a wide range of instrumentation to monitor and analyse its contents. In contrast with experiments in the atmosphere, CLOUD can compare processes when the cosmic ray beam is present and when it is not. In this way cosmic ray-aerosol-cloud microphysics can be studied under carefully controlled laboratory conditions.

2.3 Apparatus

2.3.1 Aerosol chamber, UV system and field cage

A schematic diagram of the pre-CLOUD experiment is shown in Fig. 1. The aerosol chamber dimensions were $2 \times 2 \times 2$ m^3. It was constructed from passivated AISI 304 stainless steel sheets in a modular design

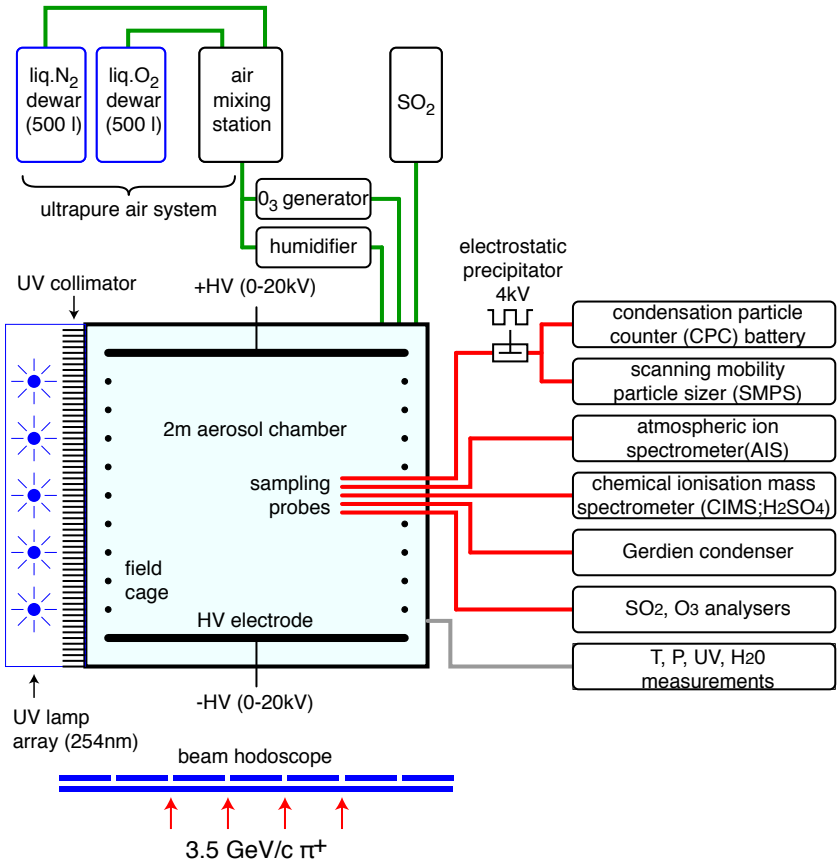

Fig. 1: Schematic diagram of the 2006 pre-CLOUD experiment.

to allow easy assembly, disassembly and transport. The sides of the chamber were sealed against a box frame with silicone O rings.

One wall of the chamber was replaced with a polytetrafluoroethylene (PTFE) window to allow the contents to be illuminated by UV light of 254 nm wavelength from a bank of seven fluorescent tubes (Philips TUV64T5 low pressure mercury vapour lamps, each 150 cm length and 75 W power). An aluminium honeycomb collimator (of 80 mm depth and 6.35 mm cell size, and painted matt black) was located between the UV lamps and the PTFE window to improve the uniformity of illumination within the chamber. With the honeycomb in place, the maximum UV intensity was 3 mW/m^2 at 254 nm wavelength. The honeycomb collimator was removed for a few special tests at higher maximum intensity (80 mW/m^2, measured at the far side of the chamber) but with poorer uniformity. The purpose of the UV light is to photo-dissociate ozone in the chamber to generate reactive oxygen and hence—in the presence of water vapour—also hydroxyl radicals. In turn the hydroxyl radicals oxidise sulphur dioxide in the chamber to form sulphuric acid.

A field cage provided electric fields of up to about 10 kV/m in the chamber. When activated, the electric field swept small ions from the chamber in about one second. The field cage comprised two 1.8×1.8 m^2 stainless steel electrodes at voltages of up +20 kV and -20 kV, respectively. The electrodes were separated by 1.8 m distance and supported at their corners by polyoxymethylene (Delrin) high voltage standoffs. One of the long hollow Delrin supports between the two electrodes contained a resistor divider chain (totalling 9.6 GΩ) to define the voltages on 23 field wires that were evenly spaced between the two electrodes and arranged along a 1.8×1.8 m^2 perimeter.

2.3.2 *Gas system*

In order to suppress contaminants (trace condensable vapours, radon and background aerosols) in the air supply for the chamber, ultrapure air was obtained from the evaporation of cryogenic liquid N_2 and liquid O_2, which were mixed in the ratio 79% and 21%, respectively. Water vapour from a Goretex tube humidifier, and trace amounts of O_3 and SO_2, were added to the inlet air. During the early runs, de-ionised water was used in the humidifier. However this was eventually replaced by Milli-Q ultrapure water [Millipore Corporation (2009)] to suppress organic contaminations. With all sampling instruments (§2.3.3) operating, the inlet air flow rate was 50 l/min to maintain a constant chamber pressure of 1.3 mbar above the ambient atmospheric pressure.

2.3.3 *Analysing instruments*

The contents of the chamber were analysed by several instruments attached to sampling probes arranged along the mid-plane of the chamber, corresponding to zero potential between the HV electrodes.

Aerosol particles were measured with a battery of five condensation particle counters (two TSI 3025 and three TSI 3010 CPCs) set to different thresholds (3, 3, 4, 7 and 9 nm). The size thresholds were calibrated in the laboratory using aerosol particles (from a nebuliser) that had been size-selected by a nano differential mobility analyser (DMA). In addition to the fast particle size measurement provided by the CPC battery, a finer-grained but slower particle size distribution was provided by a scanning mobility particle sizer (SMPS). However, due to space constraints, a long sampling line had to be installed for the SMPS and so transmission losses imposed an effective threshold of about 20 nm.

Ions and charged aerosols were measured with a Gerdien condenser, air ion spectrometer (AIS) and electrostatic precipitator placed in the inlet line of the CPC battery. The precipitator was switched between two levels (0 and 4 kV) every 40 s to measure the total and uncharged aerosol concentrations, respectively. The AIS [Mirme et al. (2007), Asmi et al. (2009)] measured the size distributions of positively charged and negatively charged particles simultaneously. The mobility range covered by the instrument is between 2.39 and 0.001 $\mathrm{cm^2V^{-1}s^{-1}}$ which correspond to mobility diameters between 0.8 and 40 nm. Each polarity has its own Differential Mobility Analyzer (DMA) divided into 21 different isolated electrometers, allowing all 21 size channels to be measured simultaneously. The measurement cycle for obtaining one positive and one negative size distribution was just over two minutes.

For part of the run, gas-phase sulphuric acid was measured with a chemical ionisation mass spectrometer (CIMS) [Möhler and Arnold (1992), Reiner et al. (1994), Curtius et al. (1998)]. The CIMS consists of an ion flow reactor coupled to a quadrupole ion trap mass spectrometer. The detection limit for H_2SO_4 is about 0.02 pptv (5×10^{-5} $\mathrm{cm^{-3}}$), for one minute time resolution. Commercial instruments were used to measure the concentrations of O_3 (Teledyne 400A) and SO_2 (Thermo 43 CTL). The chamber was instrumented with sensors to measure temperature, pressure, relative humidity and UV intensity.

2.3.4 *CERN PS T11 beam*

The detector was installed on the T11 beamline in the East Hall at the CERN PS. During selected periods, the chamber was exposed to a 3.5 GeV/c π^+ beam from a secondary target. Pions of this energy correspond closely to the characteristic ionisation of cosmic ray muons penetrating the lower troposphere. The beam intensity, horizontal profile and vertical profile were measured by a plastic scintillation counter hodoscope of overall size 140×140 cm^2, comprising 7 vertical counters of 140×20 cm^2 followed by 7 horizontal counters of the same dimensions. The beam optics were adjusted to provide a wide transverse profile; the beam size in the chamber was about 1×1.2 m^2 ($h \times v$).

The beam intensity could be adjusted to provide equilibrium ion-pair (i.p.) concentrations in the chamber of up to about 10,000 i.p. $\mathrm{cm^{-3}}$ (§2.4.1), which is about a factor 10 higher than typical atmospheric concentrations in the lower troposphere. Any intermediate setting between this maximum and

the cosmic ray background level could be reached by adjusting the beam collimators. With no beam and the clearing field on, the ion pair concentration could be further reduced, reaching about 1 i.p. cm^{-3} at 20 kV/m.

2.4 Results

2.4.1 Ion pair concentration vs. beam intensity

We will provide here a simple estimate of the expected ion pair concentration in the chamber as a function of beam intensity, in order to make a comparison with the experimental measurements. Assuming low aerosol concentrations in the chamber, the evolution of the concentration of positive or negative ions, $n_{\pm}$ [cm^{-3}] is given by [Tammet et al. (2006)]

$$\frac{dn_{\pm}}{dt} = Q - \alpha n_{\pm}^2$$

where Q [$\mathrm{cm}^{-3}\mathrm{s}^{-1}$] is the ion-pair production rate and α [1.6×10^{-6} $\mathrm{cm}^3\mathrm{s}^{-1}$] [Tammet et al. (2005)] is the ion-ion recombination coefficient. At equilibrium, $dn_{\pm}/dt = 0$ and

$$n_{\pm} = \sqrt{Q/\alpha} \tag{1}$$

Galactic cosmic rays traversing the chamber produce a mean ionisation rate, Q_c = 4 i.p. $\mathrm{cm}^{-3}\mathrm{s}^{-1}$ [Tammet et al. (2006)]. From Eq. 1, this would be expected to result in an equilibrium ion pair concentration at zero beam intensity, $n_{\pm} = \sqrt{4/1.6 \times 10^{-6}} = 1600$ cm^{-3}, in the absence of any losses other than ion-ion recombination. The ion pair lifetime due to ion-ion recombination is $\tau = 1/\sqrt{\alpha Q} = 400$ s. Diffusion losses of ions to the chamber walls are significant on this time scale and so will reduce the equilibrium ion concentration below 1600 cm^{-3}. Moreover, the presence of a pre-existing aerosol population will also create an ion sink and significantly decrease the ion concentration.

When the accelerator beam is present, there is an additional ionisation rate, Q_b, that is directly proportional to the mean beam rate, N_b [s^{-1}]. Making the simple assumption that the ion pairs created within the limited ($\sim$1 m) aperture of the beam are uniformly diluted over the entire chamber volume by diffusion and air flow,

$$Q_b = N_b \, I \, l \, / \, V \tag{2}$$

where I = 61 i.p. cm^{-1} is the mean ionisation per cm for a 3.5 GeV/c π^+ in air at s.t.p. [Smirnov (2005)], l = 200 cm is the path length of a beam particle in the chamber, and $V = 8 \times 10^6$ cm^3 is the chamber volume. Equation 2 therefore provides the following relationship between mean ion pair production rate in the chamber and beam intensity

$$Q_b = 1.5 \times 10^{-3} \, N_b \tag{3}$$

The maximum beam rate in the CERN T11 beamline is $N_b^{max} \sim 220$ kHz, which indicates a maximum ionisation rate, $Q_b^{max} = 330$ $\mathrm{cm}^{-3}\mathrm{s}^{-1}$. This is about a factor 100 higher than the ionisation rate from galactic cosmic rays. From Eq. 1, this is expected to result in an equilibrium ion pair concentration, $n_{\pm} = \sqrt{330/1.6 \times 10^{-6}} = 14,000$ cm^{-3}. In practice the mean ion concentration in the chamber will be smaller since ion losses other than ion-ion recombination have been ignored. In particular, diffusive losses of ions to the walls of the chamber are important, as well as ion scavenging by aerosols.

The experimental measurements are shown in Fig. 2. The simple estimates above are in good agreement with the experimental data, namely ion pair concentrations ranging from about 1500 cm^{-3} at zero beam to about 12,000 cm^{-3} at the maximum, and a square root dependence on beam intensity. The peak concentrations are somewhat lower than the estimate above, as expected.

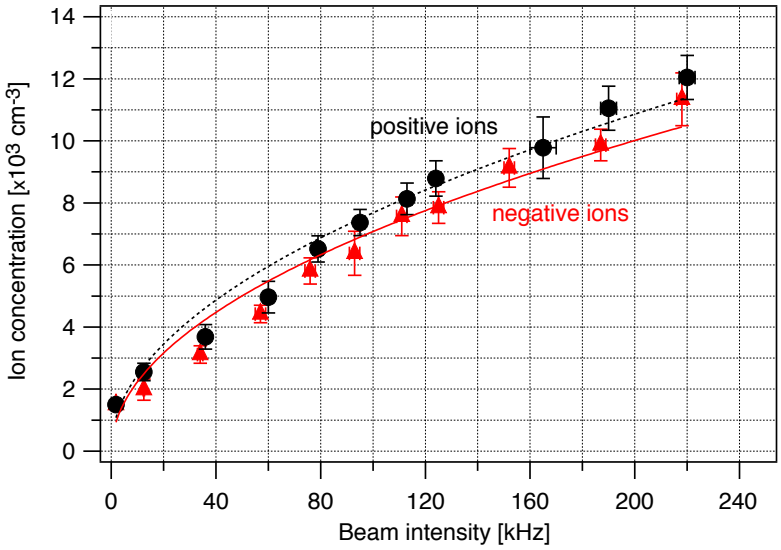

Fig. 2: Ion concentration in the chamber, measured with the Gerdien counter, as a function of beam intensity for i) positive ions (black circles and dashed curve) and ii) negative ions (red triangles and solid curve), under low aerosol background conditions (2–60 cm^{-3}, in a size range near 3 nm). The fitted curves are of the form $n_{\pm} = k_1\sqrt{N_b} + k_0$, where k_i are free parameters. The finite ion concentrations at zero beam intensity are due to galactic cosmic rays.

2.4.2 Nucleation events

2.4.3 Determination of nucleation and growth rates

We used the size distribution from the AIS to calculate the formation and growth rates of charged particles. The AIS measures ions in the mobility diameter range 0.9–42 nm, so we are able to detect the appearance of the newly formed particles at around 2 nm size and monitor their subsequent growth (an example of the AIS spectra is shown in Fig. 3). Here the population of newly formed particles is taken to be those in the size range 2–3 nm. The formation rate of charged aerosol particles at 2 nm size threshold, $J_2^{\pm}$ [$\mathrm{cm}^{-3}\mathrm{s}^{-1}$], is given by [Kulmala et al. (2007)]

$$J_2^{\pm} = \frac{dN_{2-3}^{\pm}}{dt} + CS_2 \times N_{2-3}^{\pm} + \frac{GR}{1\,nm} N_{2-3}^{\pm} + \alpha N_{2-3}^{\pm} N_{<3}^{\mp} - \beta N_{2-3} N_{<3}^{\mp} \tag{4}$$

where the superscript $\pm$ refers to positively and negatively charged particles, respectively, the subscript <3 indicates particles below 3 nm diameter, N_{2-3} [cm^{-3}] is the particle concentration in the 2–3 nm range, CS_2 [s^{-1}] is the coagulation sink rate for 2-nm particles [Kulmala et al. (2001)], GR [$\mathrm{nm\,s}^{-1}$] is the particle growth rate, α [1.6×10^{-6} $\mathrm{cm}^3\mathrm{s}^{-1}$] is the ion-ion recombination coefficient [Tammet et al. (2005)], and β [$\mathrm{cm}^3\mathrm{s}^{-1}$] is the ion-neutral attachment coefficient.

Particle growth rates were determined from the AIS size spectra by finding the peak position in each channel of the AIS in the 2–5 nm region as a function of time, and then fitting a linear equation to these points. Further details of this method can be found in [Hirsikko et al. (2005)].

In the case of all aerosol particles (charged plus neutral), the formation rate of 3 nm particles, J_3 [$\mathrm{cm}^{-3}\mathrm{s}^{-1}$], is [Kulmala et al. (2007)]

$$J_3 = \frac{dN_{3-4}}{dt} + CS_3 \times N_{3-4} + \frac{GR}{1\,nm} N_{3-4} \tag{5}$$

Here, particle growth rates were determined from the CPCs. We assume that the coagulation sink losses with larger-sized particles are negligible since their concentrations were relatively low. Also, typical co-

agulation rates between 3 nm and, for example, 10 nm particles are around $10^{-8}\ \mathrm{s}^{-1}$ and thus negligible. Therefore, the formation rate is simply

$$J_3 = \frac{dN_{>3}}{dt}$$

Overview of nucleation events: During the 4-week run, 44 nucleation bursts were observed, with formation rates of particles above the 3 nm detection threshold between 0.1 and 100 $\mathrm{cm}^{-3}\mathrm{s}^{-1}$, and growth rates between 2 and 37 $\mathrm{nm\,h}^{-1}$. These values are similar to those observed in the atmosphere [Kulmala et al. (2004)], e.g. growth rates of 1–2 $\mathrm{nm\,h}^{-1}$ in the boreal forest [Dal Maso et al. (2005)], and 40 $\mathrm{nm\,h}^{-1}$ in Mexico City [Iida et al. (2008)]. However, the measured $\mathrm{H_2SO_4}$ concentrations of around $10^6\ \mathrm{cm}^{-3}$ or less were insufficient to support growth rates above 0.1 $\mathrm{nm\,h}^{-1}$, and so additional condensable vapours must have been present in the chamber. Although their identity is unknown, the early runs showed strong nucleation bursts in association with high $\mathrm{O_3}$ concentrations and in the absence of UV light, which indicates the presence of organic vapours.

The contribution of ion-induced nucleation to the aerosol bursts can be revealed in two independent ways: 1) the presence of a high fraction of charged aerosols in the event, and 2) association of a change of the beam intensity immediately followed by a change of nucleation rate, and a dependence of the nucleation rate on beam intensity. Each of these is discussed below.

Events with a high charged fraction: The presence or absence of ion induced nucleation can be in principle be determined by measuring the charged vs. neutral fractions of the aerosol population as a function of size. Even in the absence of ion induced nucleation, a finite charged fraction is expected due to diffusion charging of neutral aerosols by small ions. A characteristic of diffusion charging is that smaller aerosols have a lower charged fraction. For example, the Boltzmann-Fuchs charging distribution predicts equilibrium charged fractions (both signs) of 1.2%, 6% and 25% for aerosols of diameter 2, 6, and 20 nm, respectively, in a bipolar ion atmosphere [Willeke and Baron (1993)]. Therefore the appearance of an "overcharged" aerosol distribution in the CPC battery—in which the charged aerosol fraction at 3 nm threshold is larger than at 7 nm threshold—is a fairly robust signature of ion-induced nucleation [Laakso et al. (2007)]. On the other hand, the *absence* of overcharging does not *exclude* contributions from ion induced nucleation, since it may indicate either that the contribution is too small to be detected or else that the initially-charged aerosols have been partly neutralised by ion-ion recombination before reaching the 3 nm size threshold for measurement.

The electrostatic precipitator (§2.3.3) on the inlet line of the CPC battery allowed the charged fractions to be compared at 3 nm and 7 nm, respectively. Of the 44 nucleation events analysed in the complete run, 6 were identified as overcharged. An example is shown in Fig. 3. During this event, the total formation rate of 3-nm particles is 3.1 $\mathrm{cm}^{-3}\mathrm{s}^{-1}$, and the charged aerosol growth rate at the start of the burst is 5.8 $\mathrm{nm\,h}^{-1}$. The CPC battery measured a charged fraction of 3% for particles between 3 nm and 5 nm, to be compared with an equilibrium charged fraction of below 2%. This suggests a small but finite contribution of ion induced nucleation.

Beam-correlated nucleation events: The second way to investigate the presence of ion induced nucleation is to keep all conditions in the chamber constant *except* for a change of pion beam intensity, and to observe a change of nucleation rate such as the onset of an aerosol burst. This of course requires the absence—or at least a low rate—of "spontaneous" aerosol bursts in the chamber. As described in §2.5.2, spurious aerosol bursts were found to be generated by small temperature increases (of order 0.1°C) of the chamber walls. This observation excludes from analysis all bursts observed in association with switching on the UV lights, since this transition always produced a substantial increase of wall temperatures (by up

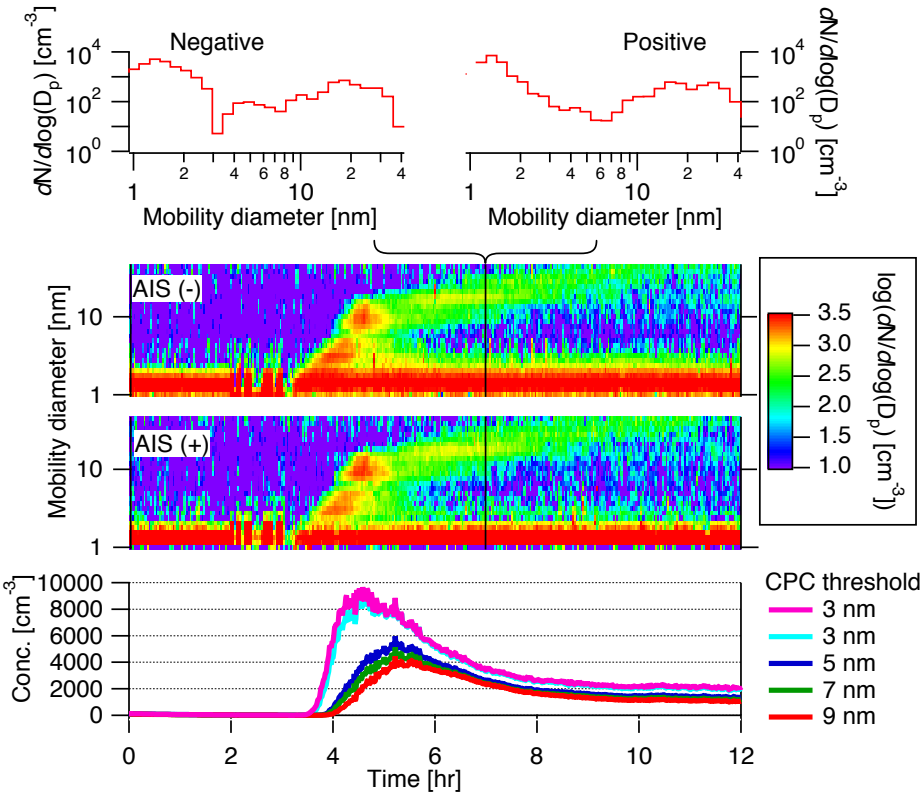

Fig. 3: An example of a nucleation burst in which ion processes are substantial. The time evolution is shown for particle size spectra measured by the CPC battery (bottom panel) and AIS (upper and middle panels for the negatively and positively charged particles, respectively). The CPCs record all neutral and charged aerosol particles, whereas the AIS records only charged aerosols and small ions. The upper histograms show size spectra of the negative (left) and positive (right) charged particles at 07h00. The aerosol size distributions are bi-modal, showing small ions and newly-formed particles below about 6 nm, and aged particles from the nucleation burst at larger sizes.

to 1°C). For this reason, all the nucleation measurements reported here involve steady illumination with UV light (2.4 mW/m^2 at 254 nm wavelength).

The clearest example of an apparent time-association of beam transitions with aerosol nucleation events was obtained in the final run of the campaign (run 35). The time evolution of various parameters for this run is shown in Fig. 4. During the entire run 35 there were stable conditions for the following parameters: $[O_3]$ = 28 ppb, relative humidity, 24%, and 254 nm UV intensity, 2.1 $\mathrm{mW\,m^{-2}}$. Initially the particle concentration was low (< 25 $\mathrm{cm^{-3}}$) but, as $[SO_2]$ was raised from 0.6 ppb to 6 ppb a strong nucleation event occurred, producing several thousand particles per cm^3. Since the clearing field was on during this interval (as can be inferred from the near-absence of small ions in the AIS data in Fig. 4), the initial aerosol burst involved only neutral nucleation. At the time when the clearing field was turned off, the particle concentration was 3600 $\mathrm{cm^{-3}}$. The beam was then immediately turned on for 2.4 h and the particle concentration increased to 4300 $\mathrm{cm^{-3}}$. (Again, the presence of beam can be inferred from the high concentration of small ions in the AIS data in Fig. 4.) The beam was then alternately turned off or on for periods of an hour or two, until the end of the run. The measured formation rates, J_3, are summarised in Table 1 and show a fair correlation with the beam intensity. The modulation pattern in Fig. 4 suggests a contribution at around the 10% level from ion induced nucleation, in addition to the dominant neutral nucleation.

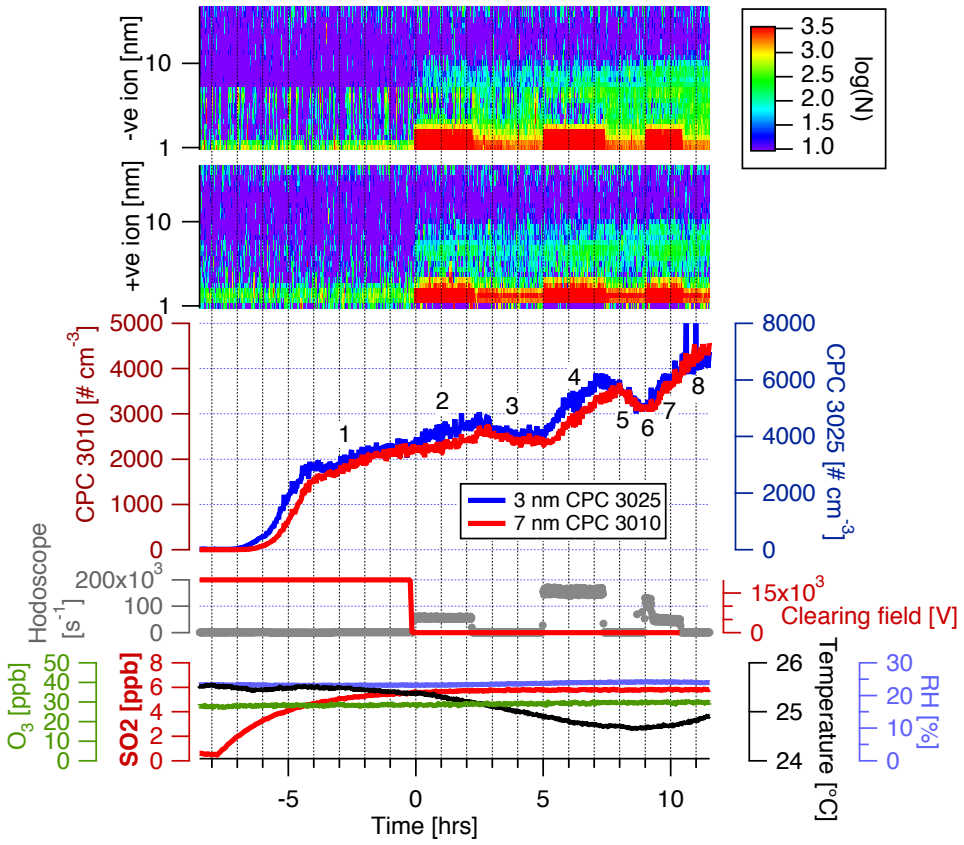

Fig. 4: Time evolution of run 35 (the final run of the experiment). A neutral nucleation burst begins about 7 h before the beam is first turned on at 00h00. Subsequently, the correlation of the beam hodoscope counts (grey curve) and the aerosol particle concentrations (red and blue CPC curves) suggests an additional component from ion induced nucleation. A zoom of the measurements from the individual instruments in the CPC battery is shown in Fig. 5. The numbered regions correspond to the aerosol formation rate measurements summarised in Table 1.

Table 1: Particle formation rates for run 35. The region numbers are shown in Fig. 4. The formation rates, J_3, correspond to the 3 nm threshold TSI 3025 CPC with a short sampling probe (magenta curve in Fig. 5). Negative values of J_3 signify a net sink of 3 nm particles.

Region no.	Start time [h]	Beam intensity [kHz]	Formation rate, J_3 [$\mathrm{cm^{-3}\,s^{-1}}$]
1	-06h30	0	0.064±0.002
2	00h00	58	0.083±0.004
3	02h20	0	-0.571±0.005
4	05h09	158	0.223±0.006
5	07h34	0	-0.163±0.009
6	09h12	116	0.400±0.030
7	09h30	50	0.133±0.046
8	10h39	0	0.076±0.015

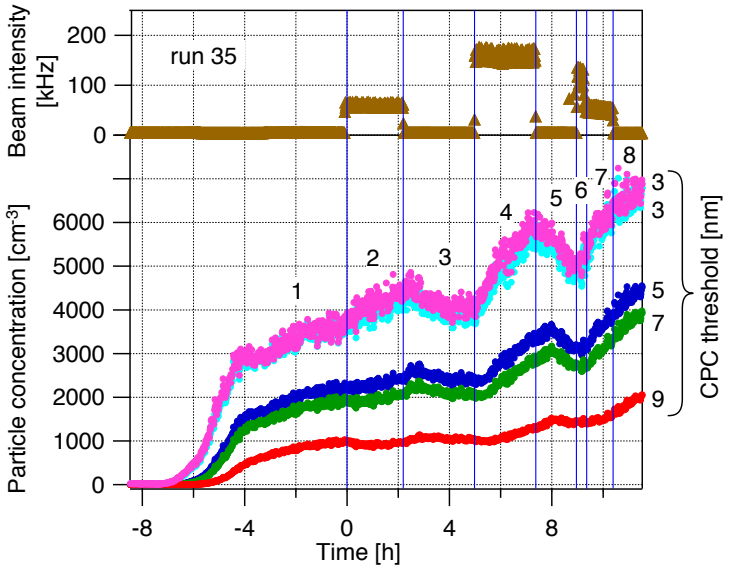

Fig. 5: Detailed time evolution of each instrument in the CPC battery during the run shown in Fig. 4 (lower panel). The aerosol concentrations appear to respond to the changes of beam intensity (upper panel), with the expected delayed response for the higher-threshold CPCs.

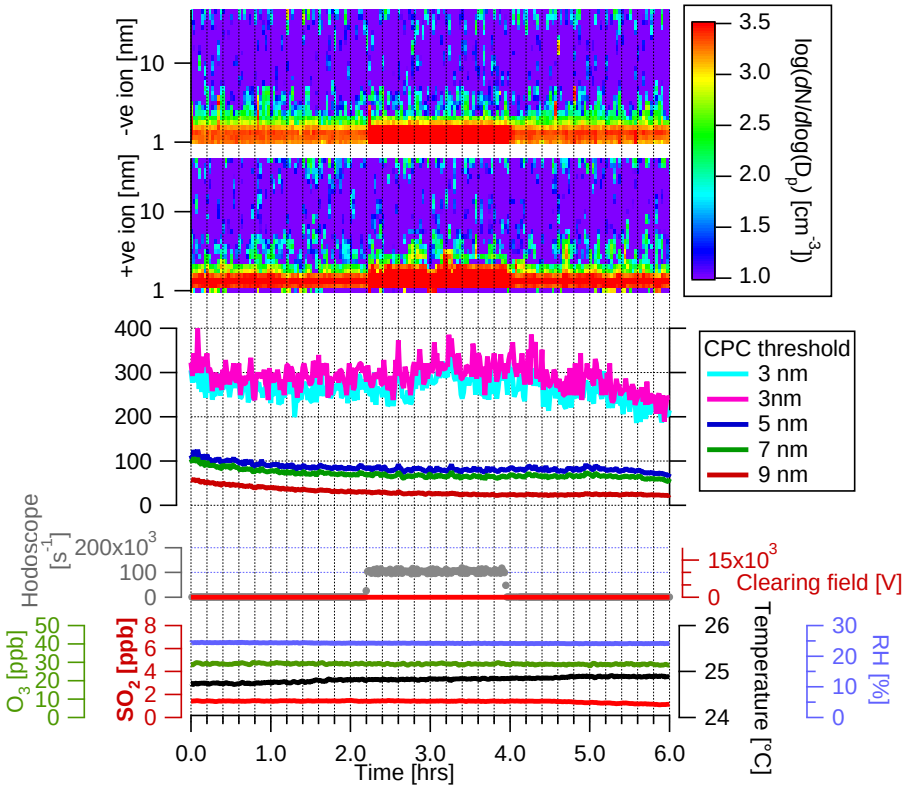

Fig. 6: Time evolution of run 28. At 2h12 the π^+ beam was turned on at 100 kHz rate (grey curve). However only a mild increase was observed in the particle concentration (magenta and cycan curves in the centre panel), indicating negligible ion induced nucleation. The other chamber conditions (including UV intensity, which is not shown) remained steady throughout this run.

The detailed time evolution of each instrument in the CPC battery during this run is shown in Fig. 5. The 3-nm CPCs respond rapidly to beam transitions whereas the 4, 7 and 9-nm CPCS show a progressively delayed response, as would be expected if the formation rate of new aerosol particles were being alternately decreased and increased. The final beam-off transition occurred during an increase of temperature of the chamber and so is subject to spurious nucleations. With the exclusion of this last transition, there is a good time-correlation of beam changes with nucleation rate changes.

Although run 35 shows a time-correlation that suggests the presence of ion-induced nucleation, there is no evidence for this from the measurements of charged fraction. As described in §2.4.3, this does not rule out the possibility of ion-induced nucleation, but neither does it add support. Furthermore other runs taken under similar conditions as run 35 show either weak or even contradictory evidence for ion induced nucleation. An example of the latter is presented in Fig. 6, which shows the time evolution of run 28. At 2h12 the beam was turned on at 100 kHz rate, which, from Eq. 3, produces in the chamber a mean ionisation rate, $Q_b = 150\ \mathrm{cm^{-3}s^{-1}}$. However, only a mild increase was observed in the particle concentration: 40 $\mathrm{cm^{-3}}$ over a two-hour period, corresponding to a formation rate of about 0.01 $\mathrm{cm^{-3}s^{-1}}$. These figures place quite a strong limit against ion induced nucleation in this event.

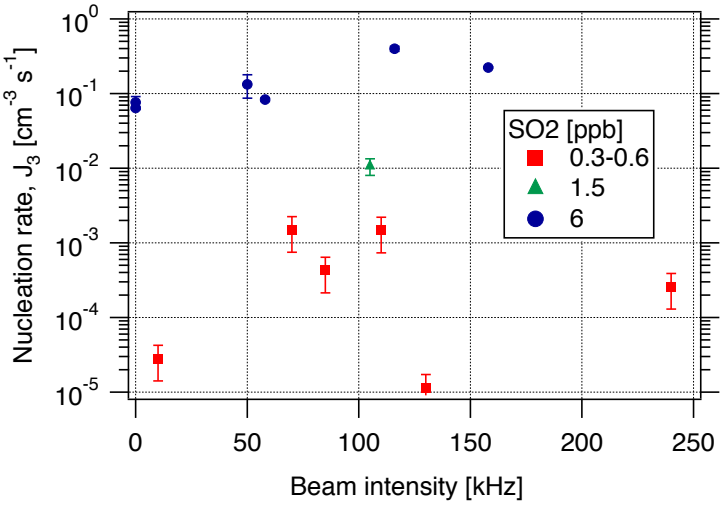

Fig. 7: Nucleation rate vs. beam intensity for several SO_2 concentrations. Where the error bars are not seen, they are smaller than the size of the data points. Although the data show no correlation with beam intensity—with the exception of the measurements taken at 6 ppb [SO_2] (see Fig. 8)—the experimental variables (such as [H_2SO_4] and background organic vapours) were not well enough controlled to exclude the presence of ion induced nucleation on the basis of this plot.

Figure 7 summarises the measurements of nucleation rate versus beam intensity for all runs taken under similar clean chamber conditions during the last week of the campaign. These data show almost no correlation with beam intensity, but do show a strong dependence of nucleation rate on [SO_2]. The measurements taken at 6 ppb [SO_2] may indicate some dependence of nucleation rate on beam intensity (Fig. 8). However, even at these relatively high SO_2 concentrations, the nucleation rate was well below 1 $\mathrm{cm^{-3}s^{-1}}$ at beam ionisation rates (Eq. 3) in the range 70–240 $\mathrm{i.p.\,cm^{-3}s^{-1}}$. So the 6 ppb [$SO_2$] measurements all show a very low ratio of nucleation rate per ion pair created in the chamber (roughly 10^{-3}). There are two possible reasons for this: either ion nucleation effects are simply unimportant or else—even at 6 ppb [SO_2]—the experimental H_2SO_4 concentration was still too low to allow significant ion-induced nucleation to occur. Unfortunately, since the CIMS was not present for these final days of data, no simultaneous [H_2SO_4] measurements are available. However, by scaling the early CIMS

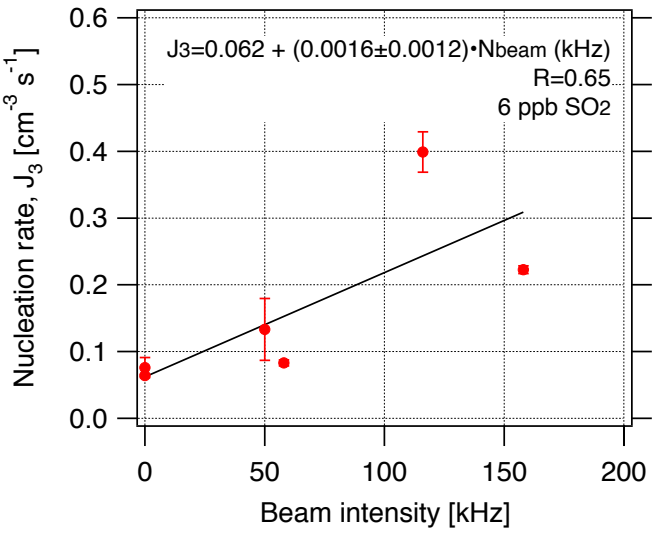

Fig. 8: Nucleation rate, J_3, vs. beam intensity, at 6 ppb $[SO_2]$. The measurements are listed in Table 1 ("negative" nucleation rates—corresponding to aerosol particle sinks—are not plotted).)

measurements, we estimate that the 6 ppb $[SO_2]$ data correspond to $[H_2SO_4] \sim 10^6$ cm^{-3}, but with large uncertainties.

In conclusion, therefore, the experimental variables were not well enough controlled to exclude the presence of ion induced nucleation on the basis of Fig. 7; it merely does not support the presence of strong contributions from this source. Indeed, at 6 ppb $[SO_2]$, there are some indications of a dependence of nucleation rate on beam intensity. As well as the poorly-known $[H_2SO_4]$, among the most important additional unknown parameters that may be affecting the measurements is the influence of background organic vapours, as described in the next section.

2.5 Technical lessons for the CLOUD design

2.5.1 Chamber cleanliness

In the early part of the 4-week experimental run, the aerosol bursts were characterised by large peak concentrations (>10,000 cm^{-3}), relatively high nucleation rates (>10 cm^{-3}s^{-1}) and rapid growth (>10 nm h^{-1}). As the run progressed and the chamber became cleaner, the aerosol bursts were significantly less intense.

The chamber was progressively cleaned by two methods: 1) continual flushing with humidified ultrapure air, and 2) cleaning cycles involving temporarily high ozone concentrations in the presence of UV light. Throughout the experiment, the air flow rate was maintained near 50 l/min. This corresponds to one chamber volume change per 160 min, which is equivalent to a dilution of gaseous impurities in the chamber by a factor of about $e^9 = 10^4$ per day. In practice, since contaminants were continually desorbing from the inner surfaces of the chamber, the rate of decrease of chamber contaminants is expected to be much slower than this. Sources of contaminants include the stainless steel walls and field cage electrodes, and organic materials such as the field cage insulators, the silicone O ring seals, the PTFE window and its sealing tape. Nevertheless, a steady reduction of contaminants was inferred from the gradually decreasing intensity of the nucleation bursts and the very low levels of background particles that were eventually achieved (well below 1 cm^{-3}).

The improving cleanliness of the chamber was also directly inferred from the ozone cleaning cycles. At the beginning of the run, 5 tests were made with $[O_3]$ in the range 100–450 ppb and with the UV lights off. Each of these elevated ozone levels caused large nucleation bursts, with peak nucleation

rates of 10 $cm^{-3}s^{-1}$ and peak concentrations in the range 1,000–17,000 cm^{-3}. No correlation was observed between the peak aerosol concentration and $[O_3]$. These observations suggest the presence of condensable organic vapours in the chamber. In contrast, later in the cycle, a similar test was performed with 440 ppb $[O_3]$—a factor of 15 higher than the nominal O_3 concentration—and no nucleation was observed. This implies a substantial reduction of organic contaminants.

Sulphur dioxide was added to the chamber only in the final days of the run. Prior to the addition of SO_2, the concentration in the chamber was measured to be steady between 0.1 and 0.2 ppb. The source of the SO_2 was not determined, but is likely to be desorption from the inner walls of the chamber, which had been exposed to atmospheric air prior to assembly. Some evidence to support this was provided by observations early in the run of increases of $[SO_2]$ by 0.1–0.2 ppb in coincidence with wall temperature increases. No correlation was observed between the intensity of the nucleation bursts and $[SO_2]$ in the range 0.1–0.2 ppb. However, when $[SO_2]$ was raised in the final days of the run, a strong correlation was observed (Fig. 7), but was not well characterised due to lack of time. The final data of the run were taken at 6 ppb $[SO_2]$.

There are several lessons from these observations for the CLOUD design. Firstly, the control and measurement of organic vapours is crucial for these experiments—not only as a potential source of backgrounds but also as a participant in the aerosol nucleation and growth processes. Secondly, the chamber components must be carefully designed and prepared to stringent standards of cleanliness, following procedures developed for UHV (ultra high vacuum) equipment. This has implications both on the selection of any material exposed to the chamber volume and also on the preparation and cleaning of the inner surfaces of the chamber and gas system. In addition, a cleaning procedure is required for the chamber between runs, including, for example, a heating and high-flush-rate cycle in the presence of UV and ozone to evaporate, oxidise and exhaust volatile surface contaminants. Concerning the generation of ultrapure air from cryogenic liquids, no contaminants were detected and so this system will be retained in the CLOUD design. This observation is, however, qualified by the limited instrumentation available for the 2006 experiment. Nevertheless, it is reassuring that—despite the relatively crude levels of cleanliness of the 2006 chamber—extremely clean experimental conditions were eventually achieved in terms of background aerosol particles ($\ll 1$ cm^{-3}) and $[H_2SO_4]$ ($\ll 10^6$ cm^{-3}).

2.5.2 Temperature stability

During the first half of the experimental run, there was no temperature control of the aerosol chamber. The chamber therefore followed the ambient temperature of the experimental hall, and the wall temperature varied in the range 20–28°C. In the second half of the run, a simple air-conditioned insulated housing was installed. This considerably improved the temperature stability, but diurnal variations of about ± 1°C remained about a mean value near 25°C.

An important observation was made from these environmentally-induced temperature changes of the chamber: a small rise of wall temperature over a short time interval almost always gave rise to a spontaneous burst of freshly-nucleated particles. Two examples are shown in Fig. 9. Bursts were observed for temperature increases as small as 0.1°C over a 15 minute period. On the other hand, temperature *decreases* did not give rise to aerosol bursts. The bursts could be unambiguously associated with wall temperature increases since no other parameters of the experiment were changed at the time of their occurrence.

Although the underlying cause of these spurious aerosol bursts was not unambiguously determined, the most likely candidate is that the temperature rise caused trace vapours (sulphur dioxide, sulphuric acid and/or organic compounds) to be released from the walls of the chamber and then nucleation occurred in the resultant relatively high vapour concentrations created in the boundary layer adjacent to the walls. Measurements during the early stage of the run—when the chamber was less clean—did indeed show evidence of increases of $[SO_2]$ during temperature increases.

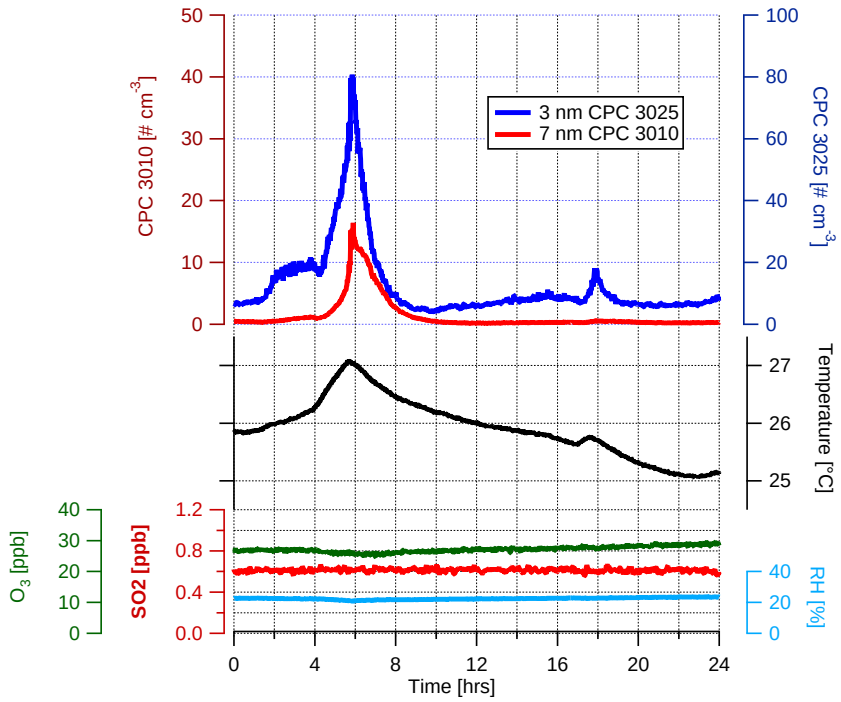

Fig. 9: Two examples of nucleation bursts (red and blue curves in the top panel) caused by small increases of the wall temperature of the aerosol chamber (black curve in centre panel).

An important consequence of this observation concerns the UV burst data, i.e. measurements of aerosol production following a brief exposure of UV light for a few minutes. The UV burst data are designed to generate a brief and limited production of H_2SO_4 in the chamber, to allow nucleation bursts to be studied under steady-state conditions of other parameters, such as ionisation rate. For practical UV intensities, these brief exposures of UV light always produced a temperature increase of the chamber wall, with a gradient of about 0.1°C per 10 minutes. In consequence all UV burst data are subject to spuriously-generated nucleations and therefore cannot be used for quantitative nucleation studies.

The lesson from these observations for the CLOUD design is that a UV system is required that provides a negligible thermal load on the chamber. The bank of UV lights for the pre-CLOUD chamber generated a thermal output of 525 W to provide a UV power of less than 0.3 W in the chamber, so there is certainly room for improvement.

2.6 Conclusions

Initial measurements have been made with a pre-CLOUD experiment at the CERN PS. The accelerator beam generated equilibrium ion pair concentrations in the aerosol chamber of between one and ten times the atmospheric values at ground level, which corresponds to between one and almost a hundred times the natural galactic cosmic ray intensities. Experimental measurements in the presence of low aerosol backgrounds confirmed a dependence of equilibrium ion pair concentrations on the square root of the beam intensity, as expected when the dominant loss mechanism is ion-ion recombination.

During the 4-week run, around 50 nucleation bursts were observed, with typical formation rates of particles above the 3 nm detection threshold of about 1–10 $\mathrm{cm^{-3}s^{-1}}$, and growth rates of 5–20 nm $\mathrm{h^{-1}}$. Concentrations of H_2SO_4 were experimentally measured with a chemical ionisation mass spectrometer to be around 10^6 $\mathrm{cm^{-3}}$ or less. The large observed growth rates indicate the presence of additional trace vapours in the aerosol chamber, whose identity is unknown but for which there is indirect evidence of

background organic vapours.

Interestingly we were able to observe different kinds of new particle formation events. A few of the events appear to be related to ion-induced nucleation and ion-ion recombination to form neutral clusters. In these cases, a significant fraction—up to around 20%—of new particle formation could be explained by ion processes. However, during most nucleation events, less than 1% of new particle formation could be explained by ion processes. The accelerator beam was also used to search for time-correlated nucleation bursts in the chambers. These revealed some evidence for a dependence of particle formation on beam intensity at the highest SO_2 concentrations of 6 ppb, although no evidence at lower concentrations.

In summary, the 2006 measurements at the CERN PS have validated the basic concept of CLOUD, provided valuable technical input for the CLOUD design and instrumentation, and provided, in some of the experiments, suggestive evidence for ion-induced nucleation of aerosol particles from trace sulphuric acid vapour at typical atmospheric concentrations.

3 CLOUD-09

3.1 Design and construction

The centrepiece of the CLOUD-09 facility (Figs. 10 and 11) is a new 3 m aerosol chamber (Figs. 12 and 13) which was designed and constructed in 2008, and is expected to arrive at CERN within the next few days. CLOUD-09 represents a large advance in performance compared with the 2006 pre-CLOUD experiment in areas such as:

- **Surface and volume cleanliness:** Trace impurities of condensable vapours must be kept at ultra-low levels (§2.5.1): well below 1 part per trillion by volume (pptv) for gaseous sulphuric acid and below 10 pptv for substances such as ammonia and condensable organics. CERN UHV procedures are being applied to all inner surfaces of the CLOUD-09 chamber and associated components (gas piping, etc.). The predominant materials are 316L stainless steel or else ceramic for the insulators; all chamber seals are metal; and no plastics are used for materials exposed to the chamber volume. The chamber is designed for bakeout at elevated temperatures (near 100°C) to evaporate volatile contaminants from the walls between experimental runs.

- **Temperature control:** Temperature fluctuations of the chamber walls of less than 0.05 °C are required (§2.5.2). A highly stable thermal control system, together with efficient thermal insulation has been designed (Fig. 10). The CLOUD-09 chamber can be operated over a large temperature range of +30°C to -90°C, corresponding to the full range of tropospheric to polar stratospheric temperatures. For bakeout, the thermal system and insulation material will operate up to near 100°C.

- **Gas system:** A new gas system has been designed for the chamber and is under construction. As before, ultrapure air is produced from cryogenic liquid N_2 and O_2 to freeze out low volatility impurities. A modeling study has been carried out to optimise the internal mixing of the chamber gases, leading to a two-fan design (Fig. 14). The trace gases are supplied on individual lines which can be isolated from the chamber and, to ensure rapid dilution, the gases enter close to the lower circulation fan (Fig. 15).

- **UV-irradiation:** A UV illumination system has been developed involving 265 vacuum-tight fibre-optic feed-throughs, evenly distributed over the top plate of the aerosol chamber. This allows for homogeneous UV illumination to conduct photolysis experiments without introducing any significant temperature change on the aerosol chamber walls and chamber contents (thermal power below 1 W).

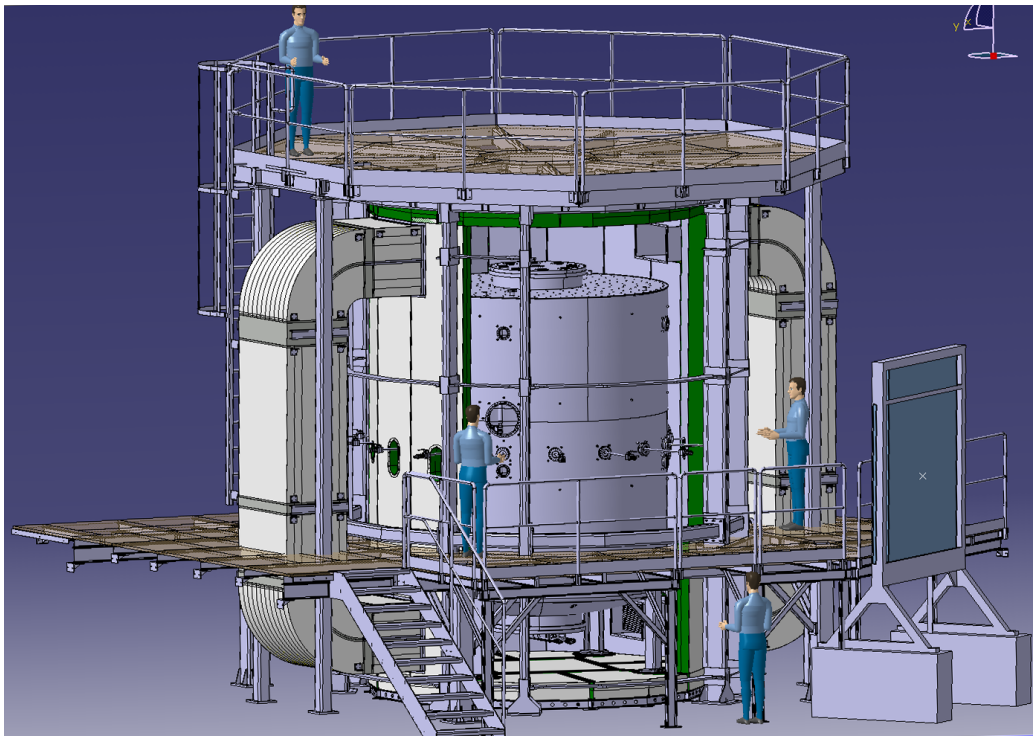

Fig. 10: The 3 m CLOUD-09 aerosol chamber and thermal housing (partially removed to show the chamber). The analysing instruments (not shown) are mounted on the platform and attached to sampling probes emerging from the mid-plane of the chamber.

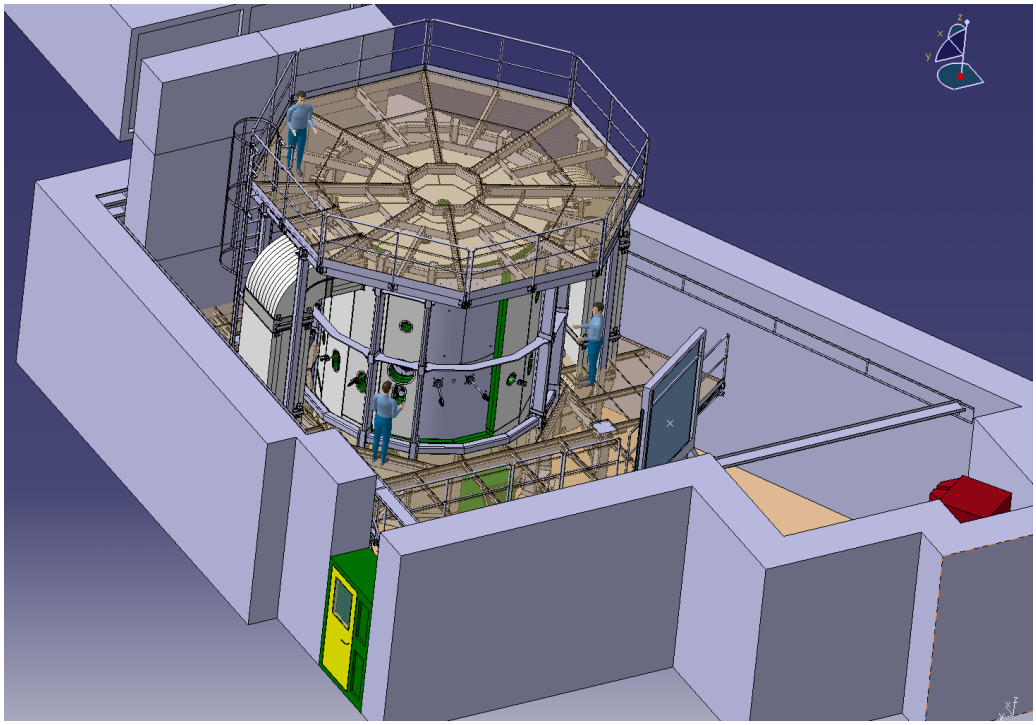

Fig. 11: Perspective of CLOUD-09 in the modified T11 experimental zone. The highly de-focussed beam emerges from the vertical dipole magnet at the bottom right of the figure and then traverses a beam hodoscope and the aerosol chamber.

Fig. 12: The 3 m CLOUD-09 chamber under construction at Kasag, Langnau, on 12 March 2009. The UV optical fibre feedthroughs and a 1 m access port can be seen on the top plate of the chamber. The ports on the walls are for sampling probes and optical windows.

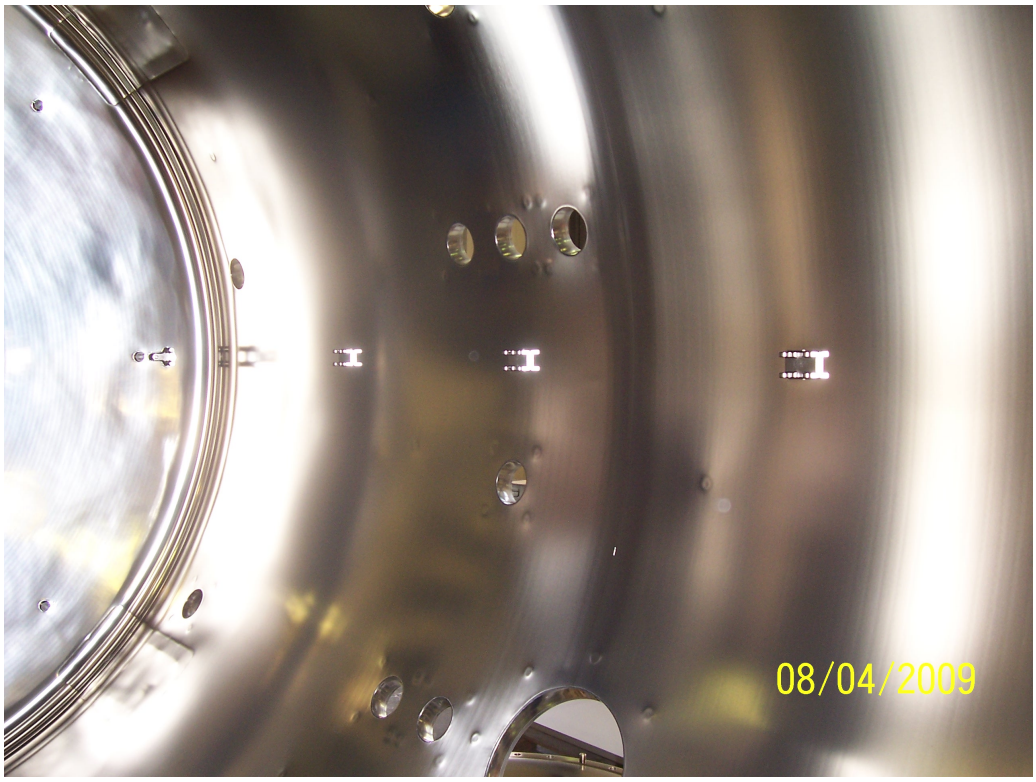

Fig. 13: Inner surface of CLOUD 3m chamber after electropolishing at Poligrat, Munich, on 8 April 2009.

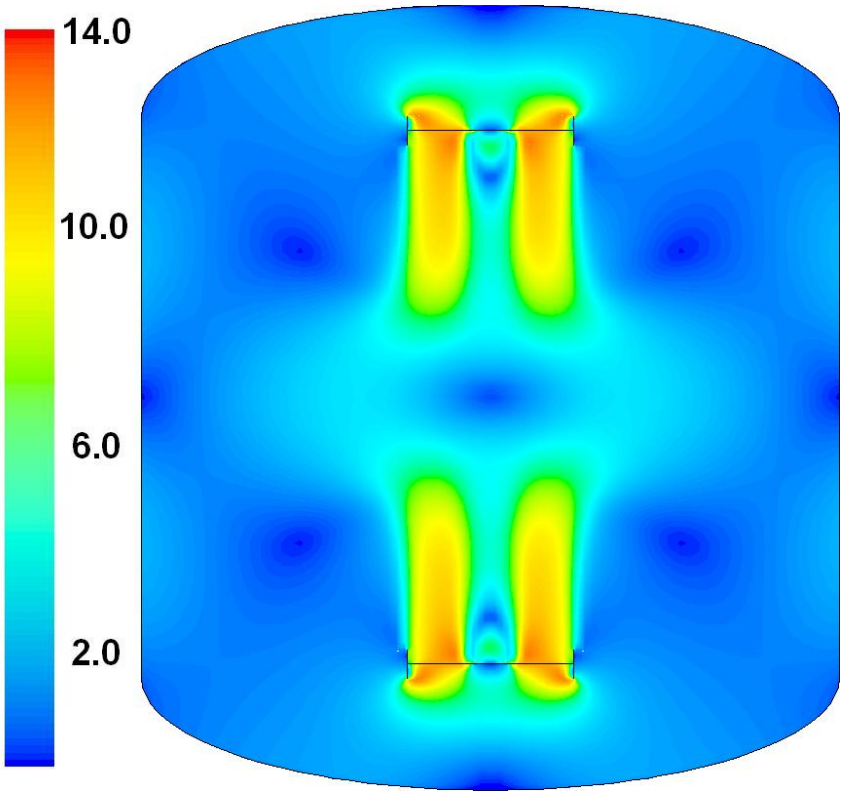

Fig. 14: Modelling study of the air velocity distribution (m/s) in the CLOUD-09 chamber resulting from two internal fans which ensure uniform gas mixing.

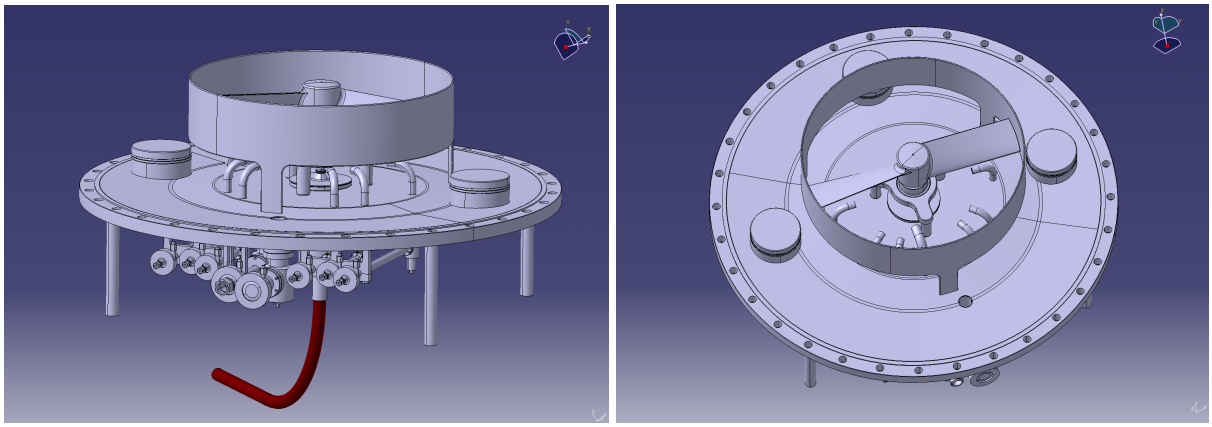

Fig. 15: Lower, 100 cm-diameter manhole cover of the CLOUD-09 chamber, showing the individual gas entry pipes, magnetically-coupled circulation fan, and instrumentation ports.

- **Field cage:** A field cage is installed inside the chamber, consisting of two transparent electrodes at up to $\pm$50 kV and an arrangement of field shaping rings in an open geometry. Great care has gone into the design of the insulating materials to guarantee the complete absence of residual charges and electric fields when the high voltage is turned off. The field cage will provide an electric field of up to 30 kV/m to remove small ions and small charged particles rapidly from the aerosol chamber.
- **Instrumentation:** The CLOUD-09 instrumentation will be considerably more advanced than before. For example, a Proton-Transfer Reaction Mass Spectrometer (PTRMS) will measure volatile organic compounds (VOCs) at the 5 pptv level, and an expansion-type Condensation Particle Counter is being developed to detect neutral aerosol particles below the 3 nm cutoff of commercial instruments, in the range that is crucial to understanding particle nucleation from trace condensable vapours.

3.2 Analysing instruments

In addition to temperature, pressure and UV sensors, the instrumentation to analyse trace gases, ions, clusters, aerosol particles, cloud droplets and ice particles in the aerosol chamber includes:

- Chemical Ionisation Mass Spectrometer (U Frankfurt)
- Frost point hygrometer (U Frankfurt)
- Ice particle analyser (U Frankfurt)
- Expansion-type Condensation Particle Counter (U Frankfurt)
- SO2 Analyser (U Frankfurt)
- Neutral cluster and Air Ion Spectrometer (U Helsinki)
- Aerosol Mass Spectrometer (U Helsinki)
- Proton-Transfer Reaction Mass Spectrometer (U Innsbruck)
- Ozone Analyser (U Innsbruck)
- Beam hodoscope (Lebedev)
- GCR monitor (Lebedev)
- High sensitivity hygrometer (IfT Leipzig)
- CCN counter (IfT Leipzig)
- NOx analyser (IfT Leipzig)
- CPC-Battery (PSI)
- Scanning Mobility Particle Sizer (PSI)
- Volatility Tandem Differential Mobility Analyser (FHNW)
- Integral Ion Counter (U Tartu)
- Mobile Size Analysing Nuclei Counter (U Vienna)
- Constant Angle Mie Scattering detector (U Vienna)

The actual instrumentation for each beam run will be selected according to the physics goals.

3.3 Experimental programme

Experiments in 2009 will be carried out near 20°C in a stable temperature environment provided by a high-precision temperature control system and chamber insulation. Then, in the 2009–2010 winter shutdown, the temperature range will be extended to the full range of tropospheric and stratospheric temperatures (-90°C to +30°C). This provides a very important experimental capability which is unavailable at most of the existing aerosol chambers and other nucleation research facilities (e.g. the Caltech aerosol chamber, the PSI aerosol chamber, the Jülich aerosol chamber and the Laminar Flow Reactor at IfT Leipzig can only be operated at ambient temperatures). Furthermore, beginning in 2010, the chamber will have the capability to act as a "cloud chamber" by making fast adiabatic pressure drops of up 100 mbar in 5 s and activating cloud droplets and ice particles.

The first two series of experiments are foreseen as:

1. **1st physics run (Sep–Nov 2009):** study of ion induced nucleation (IIN) for various H_2SO_4, H_2O, and ion concentrations at room temperature; comparison with neutral nucleation conditions.
2. **2nd physics run (Spring 2010):** IIN for various H_2SO_4, H_2O and ion concentrations at variable temperatures and with NH_3 or volatile organic compounds (VOCs) as additional parameters.

An important part of these early measurements will be to characterise the technical performance of the CLOUD-09 chamber in areas such as background contaminants, temperature stability, reproducibility of aerosol burst measurements, trace gas lifetimes, etc.

4 SCHEDULE AND BEAM REQUEST FOR 2009

The requested T11 periods in 2009 are as follows:

1. Technical run, 8wk (22Jun - 13 Aug):
   - Chamber cleaning and evaluation
   - System tests (gas system, thermal control, field cage, UV, circulation fans, DAQ)
   - Instrument tests and commissioning
   - Beam hodoscope, GCR counters, beam optics tuning, ion characterisation in chamber
   - No trace gases added to chamber, so no nucleation events expected
2. Physics run, 9wk (21Sep - 22Nov):
   - Setup period, 3wk (21Sep - 11Oct)
   - Physics data, 4 wk (12Oct - 8Nov)
   - Buffer period, 2wk (9Nov - 22Nov)

There is a great deal of work to be done in 2009 to complete the CLOUD-09 construction and to commission the detector and start physics. During the Technical run, CLOUD will make very light use of the beam since we will be commissioning a lot of new equipment, involving personnel in the T11 zone. During the physics run, we hope to be steady users of the beam. Furthermore, from now until the end of the year, we will essentially require full-time access to the T11 zone to install and commission CLOUD-09.

Acknowledgments

The CLOUD collaboration would like to thank P. Minginette for his outstanding CLOUD design work. In addition, M. Lazzaroni, L. Gatignon and I. Efthymiopoulos are thanked for their efficient work in carrying out the T11 modifications. We would also like to thank many CERN specialists for their invaluable contributions to CLOUD, including S. Atieh, A. Braem, J. Baechler, G. Favre, L. Ferreira, M. Guinchard, S. Haider, R. Kristic, S. Mathot and M. Wilhelmsson.

References

[Asmi et al. (2009)] Asmi, E., Sipilä, M., Manninen, H.E. , Vanhanen, J., Lehtipalo, K., Gagné, S., Neitola, K., Mirme, A., Mirme, S., Tamm, E., Uin, J., Komsaare, K., Attoui, M. and Kulmala, M., Results of the first air ion spectrometer calibration and intercomparison workshop. Atmos. Chem. Phys., 9, 141-154, 2009.

[Carslaw, Harrison and Kirkby (2002)] Carslaw, K.S., Harrison, R.G., and Kirkby, J., Cosmic rays, clouds, and climate, Science, 298, 1732–1737, 2002.

[CLOUD Collaboration (2000, 2004, 2006)] CLOUD Collaboration: A study of the link between cosmic rays and clouds with a cloud chamber at the CERN PS, CERN-SPSC-2000-021 (2000); CERN-SPSC-2000-030 (2000); CERN-SPSC-2000-041 (2000); CERN-SPSC-2004-023 (2004); CERN-SPSC-2006-004 (2006), available at: `http://cloud.web.cern.ch/cloud/`, 2009.

[Curtius et al. (1998)] Curtius, J., Sierau, B., Arnold, F., Baumann, R., Busen, R., Schulte, P., and Schumann, U., First direct sulphuric acid detection in the exhaust plume of a jet aircraft in flight, Geophys. Res. Lett., 25, 923, 1998.

[Dal Maso et al. (2005)] Dal Maso, M., Kulmala, M., Riipinen, I., Wagner, R., Hussein, T., Aalto, P.P., and Lehtinen, K.E.J., Formation and growth of fresh atmospheric aerosols: eight years of aerosol size distribution data from SMEAR II, Hyytiälä, Finland, Boreal Env. Res., 10, 323–336, 2005.

[Enghoff and Svensmark (2008)] Enghoff, M.B., and Svensmark, H., The role of atmospheric ions in aerosol nucleation - a review, Atm. Chem. Phys., 8, 4911–4923, 2008.

[Hirsikko et al. (2005)] Hirsikko, A., Laakso, L., Hörrak, U., Aalto, P. P., Kerminen, V.-M., Kulmala, M. Annual and size dependent variation of growth rates and ion concentrations in boreal forest. Boreal Env. Res., 10, 357369, 2005.

[Iida et al. (2008)] Iida, K., Stolzenburg, M.R., McMurry, P.H., and Smith, J.N., Estimating nanoparticle growth rates from size-dependent charged fractions: analysis of new particle formation events in Mexico City, J. Geophys. Res., 113, D05207, doi:10.1029/2007JD009260, 2008.

[IPCC (2007)] IPCC, Climate Change 2007: the Physical Science Basis. Contribution of Working Group I to the Fourth Assessment Report of the Intergovernmental Panel on Climate Change, Cambridge University Press, 2007.

[Kazil, Harrison and Lovejoy (2008)] Kazil, J., Harrison, R.G., Lovejoy, E.R., Tropospheric new particle formation and the role of ions, Sp. Sc. Rev., 137, 241–255, (2008).

[Kirkby (2007)] Kirkby, J., Cosmic rays and climate, Surv. Geophys., 28, 333–375, 2007.

[Kulmala et al. (2001)] Kulmala, M., Dal Maso, M., Mäkelä, J.M., Pirjola, L., Väkevä, M., Aalto, P.P., Miikkulainen, P., Hämeri, K., O'Dowd C.D., On the formation, growth and composition of nucleation mode particles, Tellus 53B, 479–490, 2001.

[Kulmala et al. (2004)] Kulmala, M., Vehkamäki, H., Petäjä, T., Dal Maso, M., Lauri, A., Kerminen, V.-M., Birmili, W., McMurry, P.H., Formation and growth rates of ultrafine atmospheric particles: A review of observations, J. Aerosol Sci. 35, 143–176, 2004.

[Kulmala et al. (2007)] Kulmala, M., Riipinen, I., Sipilä, M., Manninen, H.E., Petäjä, T., Junninen, H., Dal Maso, M., Mordas, G., Mirme, A., Vana, M., Hirsikko, A., Laakso, L., Harrison, R.M., Hanson, I., Leung, C., Lehtinen, K.E.J., Kerminen, V.-M., Toward direct measurement of atmospheric nucleation, Science 318, 89–92. 10.1126/science.1144124, 2007.

[Laakso et al. (2007)] Laakso, L., Gagné, S., Petäjä, T., Hirsikko, A., Aalto, P.P., Kulmala, M., and Kerminen, V.-M., Detecting charging state of ultra-fine particles: instrumental development and ambient measurements, Atm. Chem. Phys., 7, 1333–1345, 2007.

[Lockwood and Fröhlich (2007)] Lockwood, M., and Fröhlich, K., Recent oppositely directed trends in solar climate forcings and the global mean surface air temperature, Proc. Roy. Soc. A, doi:10.1098/rspa.2007.1880, 2007.

[Millipore Corporation (2009)] Millipore Corporation, Massachusetts, USA. `http://www.millipore.com/index.do/`, 2009.

[Mirme et al. (2007)] Mirme, A., Tamm, E., Mordas, G., Vana, M., Uin, J., Mirme, S., Bernotas, T., Laakso, L., Hirsikko, A., and Kulmala, M.: A wide range multi-channel Air Ion Spectrometer, Boreal Env. Res., 12, 247264, 2007.

[Möhler and Arnold (1992)] Möhler, O., and Arnold, F., Gaseous sulfuric-acid and sulfur-dioxide measurements in the Arctic troposphere and lower stratosphere - implications for hydroxyl radical abundances, Berichte Der Bunsen-Gesellschaft - Physical Chemistry Chemical Physics, 96, 3, 280–283, 1992.

[Reiner et al. (1994)] Reiner, T., and Arnold, F., Laboratory investigations of gaseous sulfuric acid formation via $SO_3 + H_2O + M \rightarrow H_2SO_4 + M$: measurement of the rate constant and products identification, J. Chem. Phys., 101, 7399–7407, 1994.

[Smirnov (2005)] Smirnov, I., Modeling of ionization produced by fast charged particles in gases, Nucl. Inst. Meth. A 554, 474–493, 2005; calculation performed with *Heed 1.01*.

[Tammet et al. (2005)] Tammet, H., Kulmala, M. Simulation tool for atmospheric aerosol nucleation bursts. J. Aerosol Sci., 36, 173196, 2005.

[Tammet et al. (2006)] Tammet, H., Hõrrak, U., Laakso, L., and Kulmala, M., Factors of air ion balance in a coniferous forest according to measurements in Hyytiälä, Finland, Atm. Chem. Phys., 6, 3377-3390, 2006.

[Willeke and Baron (1993)] Willeke, K., and Baron, P.B., Aerosol Measurements; Principle, Techniques, and Applications, Van Nostrand Reinhold, New York, ISBN 0-442-00486-9, 1993.